



Davis Joel M. (Orcid ID: 0000-0003-3522-7910)
Grindrod Peter Martin (Orcid ID: 0000-0002-0934-5131)
Boazman Sarah J. (Orcid ID: 0000-0003-4694-0818)

Quantified Aeolian Dune Changes on Mars Derived from Repeat Context Camera Images

Joel M. Davis¹, Peter M. Grindrod¹, Sarah J. Boazman^{1,2}, Pieter Vermeesch², Thomas Baird²

¹Department of Earth Sciences, Natural History Museum, London, SW7 5BD, UK

²Department of Earth Sciences, University College London, London, WC1E 6BT, UK

Corresponding author: Joel Davis (joel.davis@nhm.ac.uk)

Key Points:

- Martian dune displacement is observed over medium- and long-term baselines (7-11 Earth years) in CTX images at six sites
- Dune migration rates and sand fluxes can be quantified in CTX using SOCET SET and COSI-Corr and compare well to results from HiRISE images
- The use of CTX has advantages and disadvantages, and the combined use of HiRISE and CTX will be beneficial

This article has been accepted for publication and undergone full peer review but has not been through the copyediting, typesetting, pagination and proofreading process which may lead to differences between this version and the Version of Record. Please cite this article as doi: 10.1029/2019EA000874

Abstract

Aeolian systems are active across much of the surface of Mars and quantifying the activity of bedforms is important for understanding the modern and recent martian environment. Recently, the migration rates and sand fluxes of dunes and ripples has been precisely measured using repeat High Resolution Imaging Science Experiment (HiRISE) images. However, the limited areal extent of HiRISE coverage means that only a small area can be targeted for repeat coverage. Context Camera (CTX) images, although lower in spatial resolution, have wider spatial coverage, meaning that dune migration can potentially be monitored over larger areas. We used time series, co-registered CTX images and digital elevation models (DEMs) to measure dune migration rates and sand fluxes at six sites: Nili Patera, Meroe Patera, two sites at Herschel crater, McLaughlin crater, and Hellespontus Montes. We observed dune displacement in the CTX images over long-term baselines (7.5-11 Earth years; 4-6 Mars years). Bedform activity has previously been measured at all these sites using HiRISE, which we used to validate our results. Our dune migration rates (0.2-1.1 m/EY) and sand fluxes (2.4-11.6 m³ m⁻¹ EY⁻¹) compare well to measurements made with HiRISE. The use of CTX in monitoring dune migration has advantages (wider spatial coverage, faster processing time) and disadvantages (ripples not resolved, DEM dune heights may be underestimated); the future combined use of HiRISE and CTX is likely to be beneficial.

Plain Language Summary

Sand dunes and ripples are present across much of the surface of Mars. The motion of both dunes and ripples has been observed from orbital satellite images and rovers on the surface, which shows that the environment is constantly changing. Previously, high-resolution (sub-meter scale) satellite images have been used to track the movement of dunes and ripples across the surface, which generally move at rates of up to several meters per year. However, the limited coverage of high-resolution images means that only select sites can be monitored. Here, we use medium resolution (meter scale) satellite images, which covers a much wider area, as a test case to see if we can accurately measure the movement of dunes, which are typically several hundred meters in length. We chose six sites that have previously been measured using high-resolution images to monitor over periods of ~ 10 Earth years. Our results show that our dune migration rates generally compare well to the high-resolution measurements. The combined future use of medium and high-resolution images for monitoring dunes on Mars is likely to be beneficial.

1 Introduction

Aeolian processes are active across much of the surface of Mars (e.g., Bourke et al., 2008; Bridges et al., 2012a) and are considered one of the predominant agents for landscape modification in non-polar regions, under the current climate conditions (e.g., Bridges et al., 2013). This is evident from the movement of aeolian bedforms (dunes and ripples) observed in high-resolution orbital images (e.g., Fenton, 2006; Bridges et al., 2012b; Silvestro et al., 2013; Banks et al., 2018; Cardinale et al., 2016; Runyon et al., 2017; Chojnacki et al., 2018; Chojnacki et al., 2019) and from landers and rovers on the martian surface (e.g., Sullivan et al., 2008; Bridges and Ehlmann, 2017). These bedforms are the result of the interaction between the surface and atmosphere and act as a record for wind regime, past and current climate, sediment availability, and erosion rates (e.g., Bridges et al., 2012b; Runyon et al., 2017; Banham et al., 2018; Chojnacki et al., 2018; Chojnacki et al., 2019; Day and Catling, 2019). Quantifying the activity of bedforms is therefore important for understanding the recent and modern martian environment.

Since 2006, the High Resolution Imaging Science Experiment (HiRISE) onboard the Mars Reconnaissance Orbiter (MRO) has been imaging Mars at 0.25 m/pixel (McEwen et al., 2007); the acquisition of high-resolution, multi-temporal orbital datasets means that bedform motion can now be monitored in numerous locations across Mars (e.g., Bridges et al., 2012; Silvestro et al., 2013; Cardinale et al., 2016; Runyon et al., 2017; Chojnacki et al., 2018; Chojnacki et al., 2019). Dune sand fluxes of $\sim 10 \text{ m}^3 \text{ m}^{-1} \text{ EY}^{-1}$ are observed in HiRISE images (e.g., Bridges et al., 2013; Chojnacki et al., 2019), comparable to some terrestrial aeolian systems (e.g., Antarctic Dry Valleys; Bridges et al., 2012b).

One method to quantitatively measure bedform displacement is to use precisely orthorectified, co-registered, and correlated time series HiRISE images using the COSI-Corr (“Co-registration of Optically Senses Images and Correlation”; Leprince et al., 2007) add-in to the ENVI (ENvironment for Visualising Images) tool suite. COSI-Corr has previously been used to monitor glacial movement on Earth (e.g., Herman et al., 2011; Heid and Kaab, 2012), fault displacement on the Earth and Mars (e.g., Hollingsworth et al., 2012; Grindrod et al., 2018), as well as bedform motion on both the Earth and Mars (e.g., Vermeesch and Drake, 2008; Vermeesch and Leprince, 2012; Scheidt and Lancaster, 2013; Silvestro et al., 2013; Bridges et al., 2012; Cardinale et al., 2016; Runyon et al., 2017).

However, the relatively small image footprint of HiRISE ($\sim 5 \text{ km}$) when compared to the size of most martian dune fields (typically tens of km), and the need for stationary interdune areas within the image for co-registration, often means that only a small area can be targeted for repeated coverage. HiRISE currently covers $\sim 2\%$ total area of the martian surface (as of early 2018; McEwen et al., 2018). While this areal coverage is a considerable achievement, the use of widely available lower spatial resolution images may complement HiRISE by providing wider context to aeolian studies. Tornebene et al (2017) used repeat ConText Camera (CTX; 6 m/pixel; Malin et al., 2007) images, oversampled to 4.6 m/pixel as a simulated product for the Color and Stereo Surface Imaging System (CaSSIS; Thomas et al., 2017) onboard the Trace Gas Orbiter (TGO), to examine dune migration in part of the Nili Patera dune field over 7.5 Earth years. Tornebene et al. observed displacement on both the lee and stoss sides of several dunes. This suggests that some dune migration can be measured in meter-scale images over long temporal baselines.

In this study, we build on the work of Tornebene et al. (2017), by using precisely orthorectified, co-registered, and correlated time series CTX images and digital elevation models (DEMs) as a test case for quantifying dune migration and sand fluxes. We selected six dune fields that are known to be active from previous measurements in HiRISE and have moderate to high dune migration rates and fluxes ($\sim 0.2\text{-}1 \text{ m/EY}$; $1\text{-}15 \text{ m}^3 \text{ m}^{-1} \text{ EY}^{-1}$; Bridges et al., 2012; Cardinale et al., 2016; Runyon et al., 2017; Chojnacki et al., 2018; Chojnacki et al., 2019): Nili Patera, Meroe Patera, two sites at Herschel crater, McLaughlin crater, and Hesperontus Montes. To validate our results, we compared our CTX measurements to HiRISE measurements from previous studies which used similar techniques. Finally, we considered the future applications of CTX in aeolian studies of Mars.

2 Study Areas

Six dune fields were selected that (1) contain bedforms known to be active from previous studies in HiRISE; (2) experience moderate to high migration rates ($> 0.2 \text{ m/EY}$) with well-defined slipfaces; (3) are covered by repeat, long temporal baseline (generally > 8 Earth years) CTX images acquired under similar imaging conditions; and (4) exhibit strong contrast between the dune and interdune (i.e., bedrock) areas. All our study sites are within the low to mid latitudes ($\sim 21.6^\circ\text{N} - 44.5^\circ\text{S}$) and mostly comprise barchan or barchanoid

dunes. All the dune fields we investigated are classified as unconsolidated and mobile (i.e., they have crisp slip face brinks) on the dune stability index of Bank et al. (2018) and Fenton and Hayward (2010).

2.1 Nili and Meroe Patera

Our main study area is the Nili Patera dune field (8.7°N, 67.3°E; Figure 1b), which contains some of the fastest known moving bedforms on Mars (~ 0.5-0.8 m/EY; 5-16 m³ m⁻¹ EY⁻¹; e.g., Bridges et al., 2012; Chojnacki et al., 2018). The Nili Patera dune field is found in the southwest quadrant of Nili Patera, a ~ 50 km wide caldera, part of the Hesperian-aged Syrtis Major Planum volcanic complex (e.g., Fawdon et al., 2015). Discrete, symmetric barchan dunes (typically 200-400 m in length) with southwest trending slip faces transition into barchanoid dunes and an eventual sand sheet across the ~ 15 km long dune field (~ 425 km²). This transition is likely driven by a decrease in downwind sand flux (Bridges et al., 2012; Ruynon et al., 2017).

We also examined the nearby Meroe Patera dune field (~ 7. 3°N, 67.7°E; Figure 1c). Meroe Patera is another volcanic caldera, ~ 50 km wide, and situated ~ 100 km southeast of Nili Patera. The Meroe Patera dune field is found on the plains outside the western boundary of the caldera and covers a larger area than the Nili Patera dune field (~ 905 km²). The dune field mostly comprises active (~ 0.5 m/EY; 17 m³ m⁻¹ EY⁻¹; Chojnacki et al., 2018) asymmetric barchan and barchanoid dunes (both typically 200-400 m in length) which trend to the southwest and have been deflected around local impact craters. Both the Nili and Meroe Patera dune fields are thought to be particularly active due to regional western wind regimes associated with the Isidis basin slopes (Chojnacki et al., 2019).

2.2 Herschel Crater

Herschel crater is a ~ 300 km Noachian impact basin (14.2°S, 129.8°E), which contains several, large (~ 10-50 km long) active dune fields and sand sheets. We investigated two of the dune fields (14.7°S, 127.9°E and 15.1°S, 131.9°E) within Herschel crater near its west and southeast rims (herein referred to as West Herschel (~ 600 km²; Figure 1d) and East Herschel (~ 100 km²; Figure 1e), respectively). These sites are ~ 225 km apart and both comprise active, south trending, asymmetric barchan and barchanoid dunes (both typically 10-300 m in length) with elongated horns which transition into sand sheets (~ 0.1-0.6 m/EY; 1-15 m³ m⁻¹ EY⁻¹; Cardinale et al., 2016; Runyon et al., 2017). At West Herschel, dunes are being funnelled through a ~ 2 km valley bound by crater ejecta and a wrinkle ridge, before they broaden out into a ~ 20 km wide dune field. The sand flux of the dunes at both sites decreases downwind, which may be influenced by the regional and local topography and changes in surface roughness (Cardinale et al., 2016; Runyon et al., 2017).

2.3 McLaughlin Crater

McLaughlin crater is a ~ 90 km Noachian impact crater in the Mawrth Vallis region of northwest Arabia Terra. We investigated the dune field (~ 160 km²) near its south rim (21.6°N, 22.6°W; Figure 1f), which is associated with a steep increase in topography and change in surface roughness caused by the impact ejecta from another nearby ~ 25 km crater, which overlies McLaughlin. The dunes comprise active, south trending, asymmetric barchans and barchanoids (both typically 10-300 m in length), which all overlie bedrock (~ 0.8 m/EY; 12 m³ m⁻¹ EY⁻¹; Chojnacki et al., 2018).

2.4 Hellespontus Montes

Our final study site was a dune field ($\sim 35 \text{ km}^2$; Figure 1g) comprising a series of westward trending barchan, barchanoid (both typically 100-250 m in length), and seif dunes (typically 5-15 km) on the eastern slopes of Hellespontus Montes, on the west margin of Hellas Planitia (44.45°S, 44.58°E). High dune migration rates here ($\sim 0.9 \text{ m/EY}$; $14 \text{ m}^3 \text{ m}^{-1} \text{ EY}^{-1}$) are associated with the Hellas basin slope winds, mid-latitude westerlies, and locally rugged terrain (Chojnacki et al., 2019). Like McLaughlin, the dunes here also all overlie bedrock.

3 Methods

We used a combination of stereo topographic data and long baseline, repeat CTX images to derive and quantify dune migration and sand fluxes following previously established methods (e.g., Bridge et al., 2012b; Ayoub et al., 2014; Chojnacki et al., 2018) in SOCET SET and COSI-Corr.

3.1 SOCET SET: DEM Production and Image Co-registration

Digital elevation models (DEMs) were produced from CTX stereo images using the USGS Integrated Software for Imagers and Spectrometers (ISIS) software and the BAE photogrammetric package SOCET SET according to the method of Kirk et al. (2008). CTX image pairs were selected such that the stereo convergence angle was $\geq 15^\circ$ degrees (defined as the difference in emission angle, taking into account the pointing direction of the spacecraft) and that images were acquired in close succession, under similar imaging conditions, and with the fewest shadows associated with the dunes. Tie points were automatically populated in SOCET SET between the two images and those occurring on dune surfaces were removed. We ran a series of bundle adjustments, removing erroneous tie points until the remaining points had an RMS pixel matching error of ≤ 0.6 pixels. The resultant DEM was then tied to Mars Orbital Laser Altimeter (MOLA; Zuber et al., 1992) topography and exported with a horizontal post spacing of 20 m/pixel and a vertical precision of ~ 1.5 -5 m (Kirk et al., 2008; Obuko et al., 2008; Sutton et al., 2015; see Table S2 in supplementary materials for calculation).

After the production of the DEM, we imported our before and after CTX images in SOCET SET (T1 and T2; assuming these were different from the S1 and S2 DEM images). Following previously established practices (e.g., Chojnacki et al., 2018), T1 and T2 images were selected to have the maximum temporal baseline available acquired under imaging conditions optimized for change detection (taken ≤ 0.1 Mars years (MY) apart and $\leq 15^\circ$ difference in incidence angle; Table S1). The T1 and T2 images were then co-registered to the DEM and exported as ortho-rectified images with a pixel size of 6 m. The use of SOCET SET in the co-registration and orthorectification process is a departure from previous methods which used COSI-Corr for this process (e.g., Bridge et al., 2012b; Ayoub et al., 2014), and our technique is similar to HiRISE methods which do not use COSI-Corr (e.g., Chojnacki et al., 2018). During trial runs, we found that SOCET SET achieved higher quality co-registration of CTX images than co-registering the images in COSI-Corr.

3.2 COSI-Corr: Image Correlation and Analysis

The CTX orthoimages were then imported into COSI-Corr, where we ran correlations using a window size of 64 x 64 pixels and a step size of 2 pixels (12 m). We found that using smaller window sizes produced noisier results (e.g., high rates of bedrock correlation misregistration). We followed standard practices by filtering our results for the effects of

spacecraft jitter and low signal to noise values (Leprince et al., 2007). The two component displacement directions (north-south and east-west) were then combined to produce a magnitude value following the robust migration direction (vector averaged) method of Nescoiu et al. (2009). We then measured the displacement of select dunes along the perceived center of the dune crest (away from any horns), which we used to calculate a migration rate. We avoided measuring dune crests that form due to a secondary wind direction, such as on the elongated horns of barchans. We then manually inspected the dune crests, lee front base and the base of the stoss for signs of change in the T1 and T2 images, as an approximate quality check to confirm displacement was occurring between the images. Manual inspection was possible for at least some of the dunes measured in COSI-Corr at each site as the changes were suprapixel. We only measured dunes that were well resolved in the DEM and avoided measuring areas adjacent to (1) significant changes in topography or shadow and (2) bedrock correlation misregistration. We also measured the average displacement of obviously static bedrock in large areas away from the dunes to determine average misregistration values as a further threshold for noise. We discarded any dunes with measured displacements below this value. Finally, we extracted elevation values from the CTX DEM to derive dune heights and therefore sand fluxes (whereby migration rate in m/EY multiplied by the dune height gives the sand flux in $\text{m}^3 \text{m}^{-1} \text{EY}^{-1}$). We report our sand fluxes as the sand flux at the dune crest as is typical for other planetary aeolian studies (e.g., Bridges et al., 2012b; Chojnacki et al., 2018, 2019). Where HiRISE DEMs were available, we also extracted elevation values along the same dune profile to compare to our CTX values.

4 Results

We measured a total of 239 dunes across the six sites (Figures 3, 4). In many examples, suprapixel displacement is clearly visible between the co-registered images at the lee front and stoss sides of the dunes (for clarity, see animations in supplementary information: Movies S1-6). As expected, no dune ripples were large enough to be resolved at any of the sites. Our displacement values of the dunes extracted from the COSI-Corr correlation contain a range of both subpixel and suprapixel values (~ 2 -15 m). These values are all significantly higher than the mean misregistration values of the adjacent interdune bedrock (~ 0.5 -1 m). In all sites, most of the measured dunes came from the upwind part of the dune field. This is because the correlation tended to break down in the downwind sections of the dune fields, where interdune bedrock was less clearly exposed and dunes were overlying sand patches. We also note that many smaller dunes were not resolved in the CTX DEM, although their displacement is clearly visible between the co-registered images (e.g. Movie S5) and in the COSI-Corr correlation.

4.1 Nili and Meroe Patera

We measured the displacement of 79 dunes across the Nili Patera dune field over a period of 9.2 Earth years (4.9 Mars years; Figures 3, 4a; S1). The measured dunes span ~ 20 km width of the dune field ($\sim 2/3$ of the total width) and extend up to ~ 5 km downwind from the most upwind dune. The mean dune displacement measured was 4.8 ± 2.4 (1σ) m. (Note that our reported mean values are given as geometric means). This mean displacement value is significantly higher than the mean bedrock misregistration value of 0.6 ± 0.5 m ($\sim 1/10$ of a CTX pixel), which was measured over an area of $\sim 200 \text{ km}^2$, away from the dunes. The mean dune migration rate is therefore 0.5 ± 0.3 (1σ) m/EY WSW. Extracting the dune heights from the CTX DTM (mean height 22.4 ± 8.8 (1σ) m) gives a mean sand flux at the dune crests of 11.6 ± 7.2 (1σ) $\text{m}^3 \text{m}^{-1} \text{EY}^{-1}$. There is significant variation in migration rates throughout the

dune field. Dunes are generally migrating at faster rates (> 0.6 m/year) in the northern and upwind areas of the dune field than the southern and downwind areas (Figure 3c).

At the nearby Meroe Patera dune field, we measured the displacement of 50 dunes over 9.5 Earth years (5.1 Mars years; Figure 4b). The measured dunes span ~ 30 km width of the dune field and extend up to ~ 3 -4 km downwind from the most upwind dune. The results are generally similar to the dunes at Nili Patera: the mean measured displacement was 5.2 ± 2.2 m (mean bedrock misregistration 0.5 ± 0.5 m), giving a mean migration rate of 0.5 ± 0.2 m/EY SW. The mean measured dune height was 17.5 ± 6.9 m, which gives a mean crest sand flux of 9.5 ± 3.6 $\text{m}^3 \text{m}^{-1} \text{EY}^{-1}$. Like at Nili Patera, the Meroe Patera dunes are generally migrating at faster rates in the northern and upwind areas (> 0.6 m/EY).

4.2 Herschel Crater

We measured the displacement of 42 dunes at the West Herschel crater site over 9.3 Earth years (4.9 Mars years; Figure 4c). At West Herschel, the measured dunes span ~ 15 km of the 20 km wide dune field and extend approximately ~ 15 km downwind from the most upwind dune measured. The mean measured displacement was 2.6 ± 0.8 m (mean bedrock misregistration 1.1 ± 0.8 m). The mean dune migration is therefore 0.3 ± 0.1 m/EY. Extracting the dune height values from the CTX DEM gives a mean height of 12.5 ± 5.1 m, which gives a mean crest sand flux of 3.6 ± 1.6 $\text{m}^3 \text{m}^{-1} \text{EY}^{-1}$. The migration rate at West Herschel generally decreases in the downwind direction and the fastest moving dunes are those being funnelled through the valley.

On the other side of Herschel crater, we measured the displacement of 12 dunes at the East Herschel crater dune field over a period of 7.8 Earth years (3.9 Mars years; Figure 4d). The measured dunes are all at the upwind end of the dune field, spanning ~ 7 km in width and extending 3 km downwind. The mean measured displacement was 4.2 ± 1.4 m (mean bedrock misregistration 0.9 ± 0.8 m). The mean dune migration is therefore 0.5 ± 0.2 m/EY SSW. This is around twice the rate of the West Herschel site. The mean measured dune height was 7.7 ± 3.1 m, which gives a mean crest sand flux of 4.2 ± 1.3 $\text{m}^3 \text{m}^{-1} \text{EY}^{-1}$. The upwind dunes are generally moving faster, however this is only from a small sample size (12 dunes). Both sites at Herschel have similar sand fluxes at their crests: ~ 4 $\text{m}^3 \text{m}^{-1} \text{EY}^{-1}$.

4.3 McLaughlin Crater

At McLaughlin crater, we measured the displacement of 26 dunes over 7.6 Earth years (4 Mars years; Figure 4e). Here, the measured dunes span ~ 15 km of the 20 km wide dune field. Like the other sites, the majority of measured dunes are at the upwind end of dune field. The mean measured displacement was 1.6 ± 0.6 m (mean bedrock misregistration 0.6 ± 0.4 m). This gives a mean migration rate of 0.2 ± 0.1 m/EY S, making the McLaughlin dunes the slowest moving of all the study sites. The mean measured dune height was 11.2 ± 5.1 m, which gives a mean crest sand flux of 2.4 ± 1.4 $\text{m}^3 \text{m}^{-1} \text{EY}^{-1}$. However, we also note that some of the smaller dunes that were not resolved in the CTX DEM (and as such were not included in our results) are moving at faster rates than our mean measured value: ~ 0.5 m/EY (Movie S5).

4.4 Hellespontus Montes

Lastly, we measured the displacement of 30 dunes at Hellespontus Montes over a period of 11.3 Earth years (6 Mars years; Figure 4f). The measured dunes span ~ 5 km in width, nearly the total width of the dune field and extend the near full length of the dune field too (bedrock is exposed throughout the entire dune field). The mean measured

displacement was 11.9 ± 4.3 m (mean bedrock misregistration 1.7 ± 2.1 m). These values give a mean migration rate of 1.1 ± 0.4 m/EY, making these the fastest dunes of all six study sites. All but one of the 30 dunes measured have migration rates higher than 0.8 m/EY. The mean measured dune height was 9.7 ± 4.5 m, which gives a mean crest sand flux of 10.2 ± 6.6 m³ m⁻¹ EY⁻¹. The high sand fluxes at the Hellespontus site are comparable to the Nili and Meroe Patera sites. There does not seem to be a trend between distance downwind and migration rates and sand fluxes.

5. Discussion

5.1 Comparison to HiRISE Dune Migration Rates and Sand Fluxes

In order to validate our approach, we first compare our mean migration rates and dune heights to previous studies that used higher spatial resolution HiRISE images (Figure 5). Our CTX-derived results generally compare well to previous measurements of the same dune fields that used similar techniques with HiRISE data. Note that as the results of previous studies were not available for individual dunes, a like-for-like comparison is not possible and some intradune variation is expected.

Our dune migration rates at Nili Patera (mean: 0.5 ± 0.3 m/EY) are similar to previous HiRISE measurements (0.5 m/EY and 0.8 ± 0.2 m/EY) by Bridges et al. (2012) and Chojnacki et al. (2018), who measured migration rates over 1.5 and 2 Mars years, respectively. Our derivation of similar results over ~ 5 Mars years suggests that dune migration rates may be relatively constant over longer periods of time. Moreover, our dune migration rates at Meroe Patera (0.5 ± 0.2 m/EY) also compare favourably to HiRISE measurements (0.5 ± 0.2 m/EY) by Chojnacki et al. (2018). We note that the mean crest sand fluxes for Nili Patera (11.6 ± 7.2 m³ m⁻¹ EY⁻¹) and Meroe Patera (9.5 ± 3.6 m³ m⁻¹ EY⁻¹) are smaller than mean measurements from HiRISE (16 ± 4.9 and 16 ± 4.5 m³ m⁻¹ EY⁻¹ for Nili and Meroe, respectively; Chojnacki et al., 2018). We address this slight discrepancy in section 5.2.

Our migration rates at West and East Herschel crater also compare favourably to HiRISE studies (Cardinale et al., 2016; Runyon et al., 2017). At the West Herschel dune field, our CTX measured migration rates (mean: 0.3 ± 0.1 m/EY) over ~ 5 Mars years are similar to HiRISE measurements (mean: 0.2 m/EY) by Cardinale et al. (2016) made over 2 Mars years. Runyon et al. (2017) measured dune migration rates at both the West and East Herschel sites, finding that the upwind dunes were moving at ~ 0.5 m/EY decreasing downwind to ~ 0.2 m/EY. These measurements are also generally similar to our CTX measurements for West and East Herschel: 0.3 ± 0.1 m/EY and 0.5 ± 0.2 m/EY, respectively. The upwind and downwind sand fluxes as measured by Runyon et al. (2017) are ~ 10 m³ m⁻¹ EY⁻¹ and 2 m³ m⁻¹ EY⁻¹, respectively. These values are similar to our mean CTX measurements West and East Herschel: 3.6 ± 1.6 m³ m⁻¹ EY⁻¹ and 4.4 ± 1.5 m³ m⁻¹ EY⁻¹, respectively.

Our migration rates for McLaughlin crater (mean: 0.2 ± 0.1 m/EY) are significantly less than HiRISE measurements (0.8 ± 0.3 m/EY) by Chojnacki et al. (2018). This difference could be explained by several factors. Dunes moving at different rates may have been measured; indeed, some of the smaller dunes not resolved in the CTX DEM (likely < 5 m in height) were moving at faster rates than 0.2 m/EY in the COSI-Corr correlation, and we did not include these in our results. Additionally, most of our measurements were concentrated up at the upwind margins of the dune field, away from some of the larger, downwind dunes. Varying rates in intradune field migration may have been caused by local variations in surface roughness or topography. The dune field at McLaughlin is found at the boundary between the McLaughlin crater floor material and impact ejecta from a superposing crater, which causes an increase in both surface roughness and topography. Furthermore, with dunes

measured at similar intervals over much of the same periods (2006-2017 vs. 2008-2016), such a discrepancy is unlikely to be due to a change in sand mobility. One final possibility to explain the discrepancies in results at this site is that different methods may produce different results. Consequently, our mean crest sand flux at McLaughlin of $2.4 \pm 1.4 \text{ m}^3 \text{ m}^{-1} \text{ EY}^{-1}$ is significantly lower than the mean sand flux of $11.5 \text{ m}^3 \text{ m}^{-1} \text{ EY}^{-1}$ by Chojnacki et al. (2018).

Our migration rates for Hellespontus (mean: $1.1 \pm 0.3 \text{ m/EY}$) compare favourably to HiRISE measurements (0.9 m/EY) by Chojnacki et al. (2019). These measurements were taken over 6 and 4.3 Mars years, respectively, suggesting that as at Nili and Meroe Patera, dune migration rates at Hellespontus may be relatively steady in the medium term. Our mean crest sand flux at Hellespontus of $10.2 \pm 6.55 \text{ m}^3 \text{ m}^{-1} \text{ EY}^{-1}$ is slightly lower than the mean sand flux of $16.8 \text{ m}^3 \text{ m}^{-1} \text{ EY}^{-1}$ by Chojnacki et al. (2019). Importantly, our results show that our CTX dune displacement measurements generally compare favourably to HiRISE measurements over a range of different scales.

5.2 CTX vs. HiRISE-Derived Dune Heights

In order to verify our CTX-derived dune heights, we compared them to HiRISE-derived heights on a per dune basis. HiRISE DEMs were publicly available (via the HiRISE PDS node) for five of our six study sites, which we manually georeferenced to the CTX DEMs. The HiRISE images used to produce the DEM were all acquired either simultaneously with the CTX images or within 0.5 Mars years, so changes in dune topography over the time in which the DEM images were acquired are unlikely to affect this comparison (Bridges et al., 2012b; Table S3). Only part of the HiRISE DEMs overlapped with the CTX measurements (34 dunes at Nili Patera; 20 dunes at West Herschel; 8 dunes at Meroe Patera; 8 dunes at Hellespontus; and 4 from each East Herschel and McLaughlin crater), but this nevertheless provided a useful comparison. Extracting the same elevation profiles from the HiRISE DEMs as we did for the CTX DEMs showed that generally the CTX values underestimated the dune height (Figure 6). On average, a CTX DEM measurement was 67% of a HiRISE DEM measurement. The East Herschel and McLaughlin sites compare particularly poorly, where the site average CTX DEM measurement is only ~40% of the HiRISE DEM measurement. However, this is only from sample size of 4 dunes per site. One explanation for the lower CTX height values is the resolution of the DEM: the slip faces of dunes at most sites are several tens of meters, which is only ~ 2-3 DEM pixels. The sudden change in height might lead to a “smoothing” effect in the DEM, meaning that the measured dune heights are less than their true values. This comparison means that our sand fluxes for the dune crests are likely underestimates of the true crest sand flux. For example, our mean crest sand flux at Nili Patera ($11.6 \pm 7.2 \text{ m}$) is less than the mean sand flux from HiRISE measurements ($16 \pm 4.5 \text{ m}$; Chojnacki et al., 2018).

5.3 Benefits, Caveats, and Considerations of using CTX

The use of CTX in monitoring dune migration and sand fluxes has advantages, despite the lower image resolution when compare to HiRISE (typically 6 vs. 0.25 m). The larger areal footprint of CTX and the potential for more repeat coverage affords a larger study area providing scope into investigate lateral and downwind variations. Figure 3 demonstrates that clear displacement maps of dune fields can be produced from CTX images with very low background noise. Additionally, CTX has a faster processing time in both SOCET SET and COSI-Corr, allowing large areas to be investigated relatively quickly. The use of CTX could

be applied to investigations into temporal dune sand flux changes, the characterization of future landing sites (Chojnacki et al., 2018), or to compare with mesoscale models of the martian climate (e.g., Hayward et al., 2009).

One limitation of our results was that measuring dunes that were well resolved in both the CTX DEM and the COSI-Corr correlation required careful consideration. We found that dunes greater than ~ 200 m (10 DEM pixels) across were generally well resolved in the DEM. However, the displacement of smaller dunes (< 100 m) that were not resolved in the DEM was still visible between the co-registered images and in the COSI-Corr correlation (e.g., Movie S5). Using alternative image pairs acquired at different times to produce the DEMs sometimes better resolved the topography of smaller dunes. Comparing to HiRISE DEMs also suggests that our CTX DEM heights may be underestimating the true height of the dune (Figure 6). Manual inspection of the DEMs is also important for quality checking as errors in the DEM could introduce false movement in the orthorectification process. Another factor is that both CTX and HiRISE COSI-Corr results can be noisy because of jitter and along the CCD seams (Ayoub et al., 2014), although this may be less of an issue for CTX because of the lower image resolution. Filtering our CTX COSI-Corr results for jitter and other forms of noise managed to remove most of these effects. We also note that the sites with strong dune-substrate albedo contrast (Nili, Meroe) produced the least noisy COSI-Corr results, whereas the sites with poor dune-substrate albedo contrast (Hellespontus) produced the noisiest results. Additionally, as the COSI-Corr correlation tended to break down in the downwind section of the dune fields because of the lack of bedrock, measuring dunes in areas where there is appropriate interdune bedrock exposure is important. Future tests of CTX could investigate dune fields with sand-starved downwind areas, such as those dune fields in Oyama and Capen craters, to produce a more representative picture of intra-dune field sand flux variations. Thus, our mean dune migration rates and sand fluxes may not be entirely representative of the variation across entire dune field, although they still provide a useful first order comparison between different sites.

The future combined use of HiRISE and CTX in dune monitoring and in COSI-Corr will likely be complementary and avoid the potential trade-offs of only using one dataset: HiRISE can quantitatively measure dune and dune ripple movement, whereas CTX can provide wider context and examine regional variation, where HiRISE coverage is unavailable. This has the advantage in that CTX is generally acquired alongside HiRISE now (often under appropriate conditions for change detection), allowing migration rates and sand fluxes to be monitored over the same time period using different data sets. In the future, the CaSSIS camera onboard TGO, which has a similar resolution to CTX (nominally 4.6 vs. 6 m), is likely to be used to monitor bedform displacement (Tornebene et al., 2017). The application of the CaSSIS's four color channels (Thomas et al., 2017) may have the potential to improve the co-registration between before and after images. We also note that the use of SOCET SET is a well-validated and mature method of image co-registration (e.g., HiRISE; Chojnacki et al., 2018) that can cope with the effects of illumination changes, which could be applied to monitoring changes in other landforms with CTX images as well (e.g., gullies, polar processes).

6 Conclusions

We used time series, co-registered CTX images and DEMs to measure dune migration and sand fluxes at six dune fields across Mars in SOCET SET and COSI-Corr: Nili Patera, Meroe Patera, West and East Herschel crater, McLaughlin crater, and Hellespontus Montes. We observed dune displacement in the CTX images over long-term baselines (7.5-11 Earth years; 4-6 Mars years), giving migration rates of 0.2-1.1 m/EY. Extracting the dune crest

heights from the CTX DEMs gives crest sand fluxes of 2.4-11.6 m³ m⁻¹ EY⁻¹. The fastest moving dunes were Hellespontus Montes, whereas those with the largest sand fluxes were Nili Patera, Meroe Patera, and Hellespontus Montes. We find that our migration rates generally compare well to previous measurements made using HiRISE, although our CTX DEM dune heights are likely to be an underestimate (and thus sand fluxes). We have shown that CTX has the potential to expand the coverage area for dune field monitoring where HiRISE is unavailable. The combined future use of both CTX and HiRISE in measuring dune changes is likely to be beneficial. Our results demonstrate that meter-scale orbital images can be used to quantify changes in aeolian systems on Mars.

Acknowledgements

JMD gratefully acknowledges UK Space Agency (UK SA) funding (ST/R002355/1). PMG acknowledges UK SA funding (ST/L00254X/1). We thank Matt Balme for reviewing a draft version of this manuscript. We thank the various Mars instrument teams for their consistent and dedicated work. We thank Matthew Chojnacki and Simone Silvestro for thorough and constructive reviews. The standard data products used here are available from the NASA PDS (<https://pds.jpl.nasa.gov/>). The CTX DEMs and co-registered time series images are available for download at <https://doi.org/10.6084/m9.figshare.c.4649537.v1>.

References

- Ayoub, F., Avouac, J. P., Newman, C. E., Richardson, M. I., Lucas, A., Leprince, S., & Bridges, N. T. (2014). Threshold for sand mobility on Mars calibrated from seasonal variations of sand flux. *Nature Communications*, 5, 1–8. <https://doi.org/10.1038/ncomms6096>
- Banham, S. G., Gupta, S., Rubin, D. M., Watkins, J. A., Sumner, D. Y., Edgett, K. S. et al. (2018). Ancient Martian aeolian processes and palaeomorphology reconstructed from the Stimson formation on the lower slope of Aeolis Mons, Gale crater, Mars. *Sedimentology*, 65(4), 993–1042. <https://doi.org/10.1111/sed.12469>
- Banks, M. E., Fenton, L. K., Bridges, N. T., Geissler, P. E., Chojnacki, M., Runyon, K. D. & Zimbelman, J. R. (2018). Patterns in Mobility and Modification of Middle- and High-Latitude Southern Hemisphere Dunes on Mars. *Journal of Geophysical Research: Planets*, 123(12), 3205–3219. <https://doi.org/10.1029/2018JE005747>
- Bourke, M. C., Edgett, K. S., & Cantor, B. A. (2008). Recent aeolian dune change on Mars. *Geomorphology*, 94(1–2), 247–255. <https://doi.org/10.1016/j.geomorph.2007.05.012>
- Bridges, N. T., & Ehlmann, B. L. (2018). The Mars Science Laboratory (MSL) Bagnold Dunes Campaign, Phase I: Overview and introduction to the special issue. *Journal of Geophysical Research: Planets*, 123(1), 3–19. <https://doi.org/10.1002/2017JE005401>
- Bridges, N. T., Ayoub, F., Avouac, J., Leprince, S., Lucas, A., & Mattson, S. (2012). Earth-like sand fluxes on Mars. *Nature*, 485(7398), 339–342. <https://doi.org/10.1038/nature11022>
- Bridges, N. T., Bourke, M. C., Geissler, P. E., Banks, M. E., Colon, C., Diniega, S., & Thomson, B. J. (2012). Planet-wide sand motion on Mars. *Geology*, 40(1), 31–34. <https://doi.org/10.1130/G32373.1>
- Bridges, N., Geissler, P., Silvestro, S., & Banks, M. (2013). Bedform migration on Mars: Current results and future plans. *Aeolian Research*, 9, 133–151. <https://doi.org/10.1016/j.aeolia.2013.02.004>

- Bridges, N., Geissler, P., Silvestro, S., & Banks, M. (2013). Bedform migration on mars: Current results and future plans. *Aeolian Research*, 9, 133–151. <https://doi.org/10.1016/j.aeolia.2013.02.004>
- Cardinale, M., Silvestro, S., Vaz, D. A., Michaels, T., Bourke, M. C., Komatsu, G., & Marinangeli, L. (2016). Present-day aeolian activity in Herschel Crater, Mars. *Icarus*, 265, 139–148. <https://doi.org/10.1016/j.icarus.2015.10.022>
- Chojnacki, M., Banks, M. E., Fenton, L. K., & Urso, A. C. (2019). Boundary condition controls on the high-sand-flux regions of Mars. *Geology*, 47(5), 427–430. <https://doi.org/10.1130/G45793.1>
- Chojnacki, M., Banks, M., & Urso, A. (2018). Wind-Driven Erosion and Exposure Potential at Mars 2020 Rover Candidate-Landing Sites. *Journal of Geophysical Research: Planets*, 123(2), 468–488. <https://doi.org/10.1002/2017JE005460>
- Day, M. D., & Catling, D. C. (2019). Potential aeolian deposition of intra-crater layering: A case study of Henry crater, Mars. *GSA Bulletin*, 1–9. <https://doi.org/10.1130/B35230.1/4719602/b35230.pdf>
- Fenton, L. K. (2006). Dune migration and slip face advancement in the Rabe Crater dune field, Mars. *Geophysical Research Letters*, 33(20), 1–5. <https://doi.org/10.1029/2006GL027133>
- Fenton, L. K., & Hayward, R. K. (2010). Southern high latitude dune fields on Mars: Morphology, aeolian inactivity, and climate change. *Geomorphology*, 121(1–2), 98–121. <https://doi.org/10.1016/j.geomorph.2009.11.006>
- Grindrod, P. M., Hollingsworth, J., Ayoub, F., & Hunt, S. A. (2018). The Search for Active Marsquakes Using Subpixel Coregistration and Correlation: Best Practice and First Results. *Journal of Geophysical Research: Planets*, 123(7), 1881–1900. <https://doi.org/10.1029/2018JE005649>
- Hayward, R. K., Titus, T. N., Michaels, T. I., Fenton, L. K., Colaprete, A., & Christensen, P. R. (2009). Aeolian dunes as ground truth for atmospheric modeling on Mars. *Journal of Geophysical Research*, 114(11), 1–11. <https://doi.org/10.1029/2009JE003428>
- Heid, T., & Käab, A. (2012). Repeat optical satellite images reveal widespread and long term decrease in land-terminating glacier speeds. *Cryosphere*, 6(2), 467–478. <https://doi.org/10.5194/tc-6-467-2012>
- Herman, F., Anderson, B., & Leprince, S. (2011). Mountain glacier velocity variation during a retreat/advance cycle quantified using sub-pixel analysis of ASTER images. *Journal of Glaciology*, 57(202), 197–207. <https://doi.org/10.3189/002214311796405942>
- Hollingsworth, J., Leprince, S., Ayoub, F., & Avouac, J. P. (2012). Deformation during the 1975–1984 Krafla rifting crisis, NE Iceland, measured from historical optical imagery. *Journal of Geophysical Research B: Solid Earth*, 117(11), 1–24. <https://doi.org/10.1029/2012JB009140>
- Kirk, R.L., Howington-Kraus, E., Rosiek, M.R., Anderson, J.A., Archinal, B.A., Becker, K.J., et al. (2008). Ultrahigh resolution topographic mapping of Mars with MRO HiRISE stereo images: Meter-scale slopes of candidate Phoenix landing sites. *Journal of Geophysical Research*, 113, E00A24, <https://doi.org/10.1029/2007JE003000>.
- Leprince, S., Ayoub, F., Klingert, Y., & Avouac, J.-P. (2007). Co-Registration of Optically Sensed Images and Correlation (COSICorr): an operational methodology for ground

- deformation measurements, in: Geoscience and Remote Sensing Symposium, 2007. *IGARSS 2007. IEEE International*, 1943–1946.
- Malin, M. C., Bell III, J.F., Cantor, B.A., Caplinger, M.A., Calvin, W.M., Clancy, R.T., et al. (2007). Context Camera Investigation on board the Mars Reconnaissance Orbiter. *Journal of Geophysical Research*, 112, E05S04. <https://doi.org/10.1029/2006JE002808>.
- McEwen, A. S., Eliason, E.M., Bergstrom, J.W., Bridges, N.T., Hansen, C.J., Delamere, W.A., et al. (2007). Mars Reconnaissance Orbiter's High Resolution Imaging Science Experiment (HiRISE). *Journal of Geophysical Research*, 112, E05S02. <https://doi.org/10.1029/2005JE002605>
- McEwen, A. S. & the HiRISE Science and Operations Team (2018). The future of MRO/HiRISE. Paper presented at 49th Lunar and Planetary Science Conference, The Woodlands, Texas. Abstract 2083.
- Necsoiu, M., Leprince, S., Hooper, D.M., Dinwiddie, C.L., McGinnis, R.N. & Walter, G.R. (2009). Monitoring migration rates of an active subarctic dune field using optical imagery. *Remote Sensing of Environment*, 113, 2441–2447. <https://doi.org/10.1016/j.rse.2009.07.004>.
- Okubo, C. H., Lewis, K. W., McEwen, A. S., & Kirk, R. L. (2008). Relative age of interior layered deposits in southwest Candor Chasma based on high-resolution structural mapping. *Journal of Geophysical Research*, 113(12), 1–15. <https://doi.org/10.1029/2008JE003181>
- Runyon, K. D., Bridges, N. T., Ayoub, F., Newman, C. E., & Quade, J. J. (2017). An integrated model for dune morphology and sand fluxes on Mars. *Earth and Planetary Science Letters*, 457, 204–212. <https://doi.org/10.1016/j.epsl.2016.09.054>
- Scheidt, S. P., & Lancaster, N. (2013). The application of COSI-Corr to determine dune system dynamics in the southern Namib Desert using ASTER data. *Earth Surface Processes and Landforms*, 38(9), 1004–1019. <https://doi.org/10.1002/esp.3383>
- Silvestro, S., Vaz, D. A., Ewing, R. C., Rossi, A. P., Fenton, L. K., Michaels, T. I., & Geissler, P. E. (2013). Pervasive aeolian activity along rover Curiosity's traverse in Gale Crater, Mars. *Geology*, 41(4), 483–486. <https://doi.org/10.1130/G34162.1>
- Sullivan, R., Arvidson, R., Bell, I. F., Gellert, R., Golombek, M., Greeley, R., & Wray, J. (2008). Wind-driven particle mobility on Mars: Insights from Mars Exploration Rover observations at “El Dorado” and surroundings at Gusev Crater. *Journal of Geophysical Research*, 113(6), 1–70. <https://doi.org/10.1029/2007JE003101>
- Sutton, S.S., Chojnacki, M., Kilgallon, A., & the HiRISE Team. (2015). Precision and accuracy of simultaneously collected HiRISE digital terrain models. Paper presented at 46th Lunar and Planetary Science Conference, The Woodlands, Texas. Abstract 3010.
- Thomas, N., Cremonese, G., Ziethe, R., Gerber, M., Brändli, M., Bruno, G., et al. (2017). The Colour and Stereo Surface Imaging System (CaSSIS) for the ExoMars Trace Gas Orbiter. *Space Science Reviews*, 212(3–4), 1897–1944. <https://doi.org/10.1007/s11214-017-0421-1>
- Tornabene, L. L., Seelos, F. P., Pommerol, A., Thomas, N., Caudill, C. M., Becerra, P., et al. (2018). Image Simulation and Assessment of the Colour and Spatial Capabilities of

the Colour and Stereo Surface Imaging System (CaSSIS) on the ExoMars Trace Gas Orbiter. *Space Science Reviews*, 214(1). <https://doi.org/10.1007/s11214-017-0436-7>

Vermeesch, P., & Drake, N. (2008). Remotely sensed dune celerity and sand flux measurements of the world's fastest barchans (Bodélé, Chad). *Geophysical Research Letters*, 35(24), 1–6. <https://doi.org/10.1029/2008GL035921>

Vermeesch, P., & Leprince, S. (2012). A 45-year time series of dune mobility indicating constant windiness over the central Sahara. *Geophysical Research Letters*, 39(14), 1–5. <https://doi.org/10.1029/2012GL052592>

Zuber, M.T., Smith, D.E., Solomon, S.C., Muhleman, D.O., Head, J.W., Garvin, J.B., et al. (1992). The Mars Observer laser altimeter investigation. *Journal of Geophysical Research*, 97, 7781–7797. <https://doi.org/10.1029/92JE00341>.

Accepted Article

Table 1: Summary table showing the mean dune heights, migration rates, and sand fluxes for the six study sites. EY and MY show the time difference between the before and after images (T1 and T2) in Earth years and Mars years respectively. The T1 and T2 images were chosen to be less than ≤ 0.1 Mars years apart, assuring the best results.

Location	T1 image central Lat. Lon.	EY	MY	Number of dunes	Dune height (m)	Migration rate (m/EY)	Sand flux ($\text{m}^3 \text{m}^{-1} \text{EY}^{-1}$)
Nili Patera	8.°N, 67.32°E	9.2	4.9	79	22.4±8.8	0.5±0.3	11.6±7.2
Meroe Patera	7.28°N, 67.75°E	9.5	5.1	50	17.5±6.9	0.5±0.2	9.5±3.6
West Herschel	15.26°S, 127.92°E	9.2	4.9	42	12.5±5.4	0.3±0.1	3.6±1.6
East Herschel	15.59°S, 131.88°E	7.8	3.9	12	7.7±3.1	0.5±0.2	4.4±1.5
McLaughlin crater	21.57°N, 22.55°W	7.6	4	26	11.2±5.1	0.2±0.1	2.4±1.4
Hellespontus	44.45°S, 44.58°E	11.3	6	30	9.7±4.9	1.1±0.4	10.2±6.55

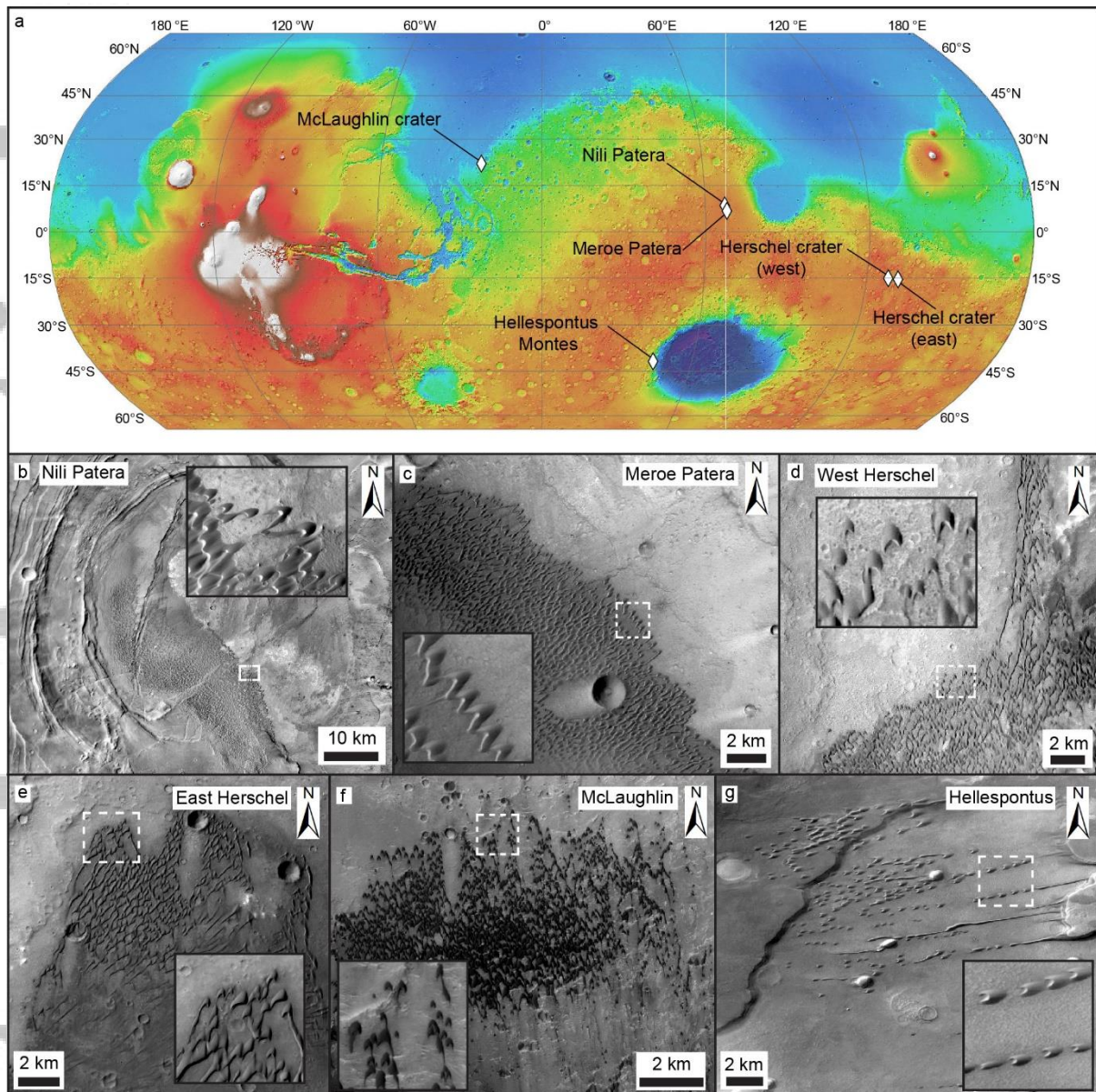


Figure 1: (a) Mars Orbital Laser Altimeter (MOLA) topographic map showing the locations of the six study areas. (b) CTX mosaic showing southwest trending barchan dunes within the caldera at Nili Patera; (c) CTX image showing southwest trending barchan dunes on the plains outside Meroe Patera; (d) CTX image showing south trending barchan dunes near the west rim of Herschel crater; (e) CTX image showing south trending barchan dunes near the east rim of Herschel crater; (f) CTX image showing south trending barchan dunes in McLaughlin crater; (g) CTX image showing west trending barchan and seif dunes in Hesperontus Montes.

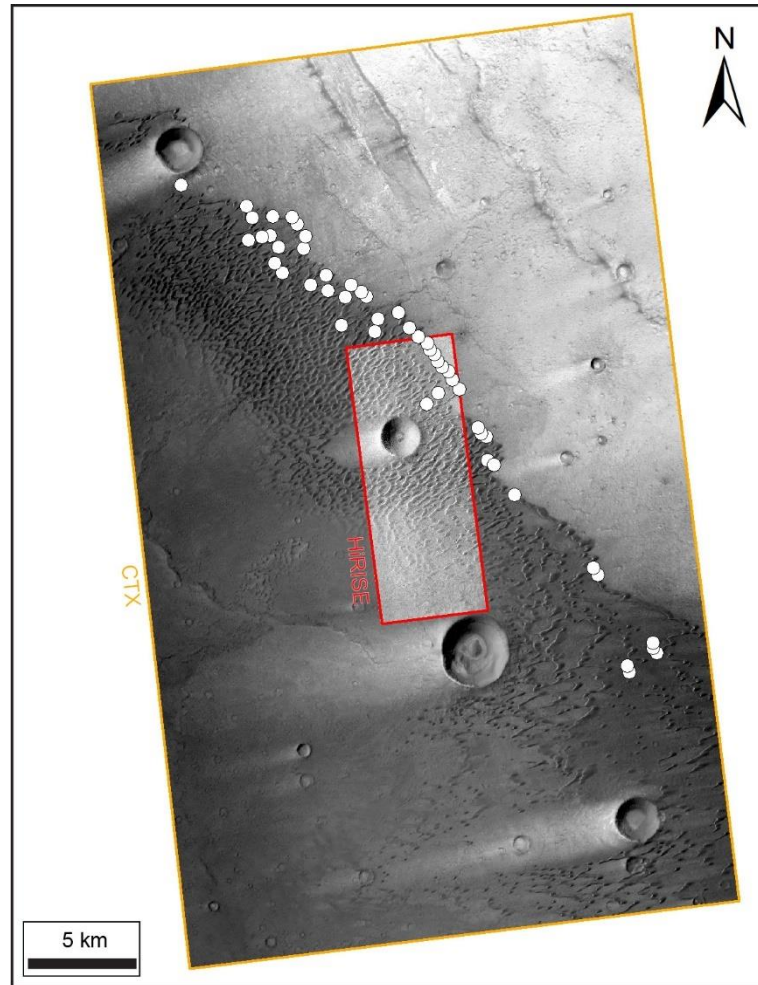


Figure 2: CTX (orange outline; P17_007754_1873_XI_07N292W) and HiRISE (red outline; PSP_007754_1875; as previously studied by Chojnacki et al. (2018)) images of the Meroe Paterra dune field. The CTX image covers a greater width of the dune field. The white circles show the measured dunes in this study.

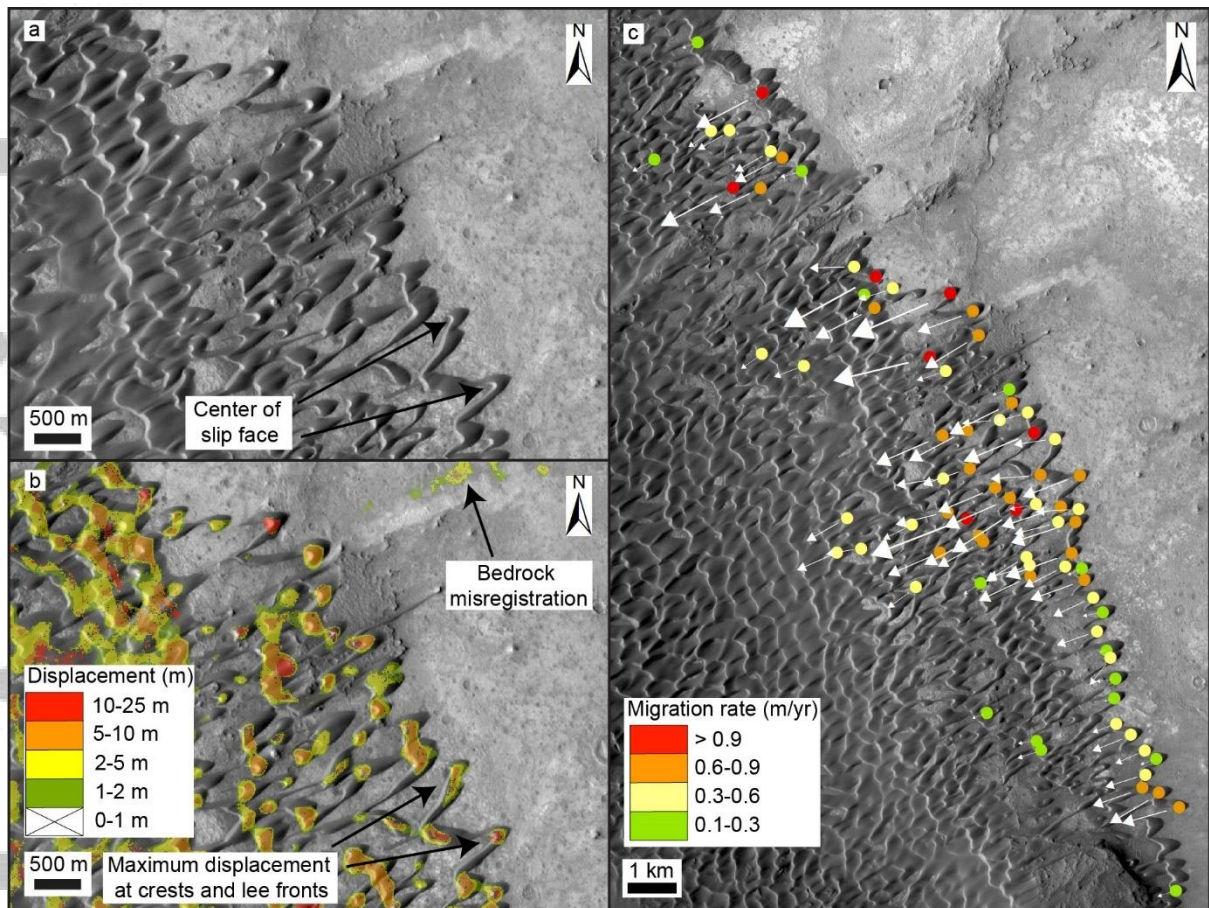


Figure 3: (a) CTX image showing part of the Nili Patera dune field, which comprises southwest trending barchan and barchanoid dunes. (b) Dune displacement values between 2007 and 2016 extracted from COSI-Corr correlation overlaid on a CTX image. (c) All measured dune migration rates for the Nili Patera dune field (mean migration rate is ~ 0.5 m/EY). Dunes are moving faster in the northern and upwind parts of the dune field. The white arrows show the dune migration direction and their size represents the migration rates of the dunes.

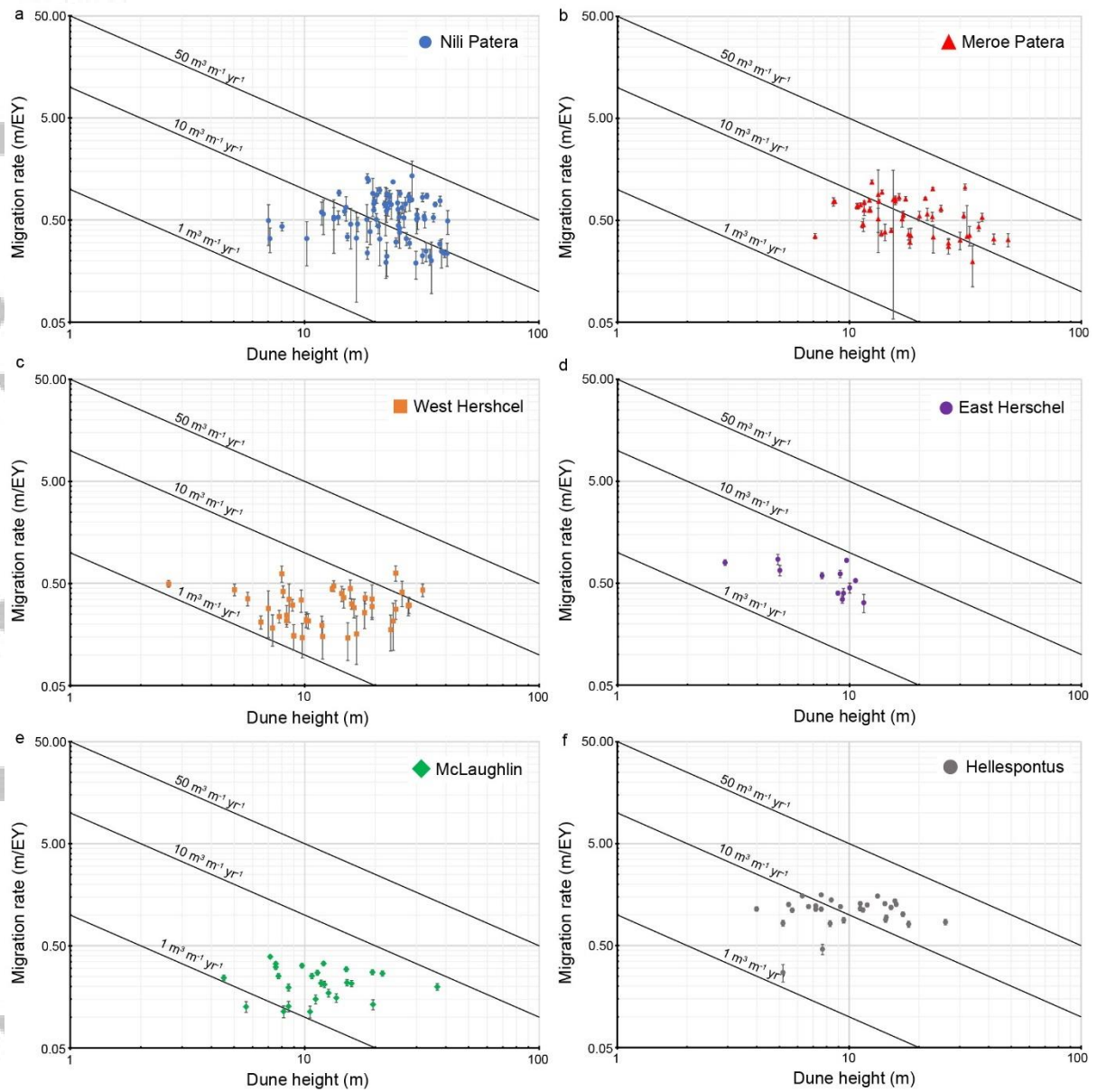


Figure 4: Log log plot showing dune height versus migration rates for our six study sites. The solid black lines show different sand fluxes at 1, 10, and 50 m³ m⁻¹ EY⁻¹, respectively.

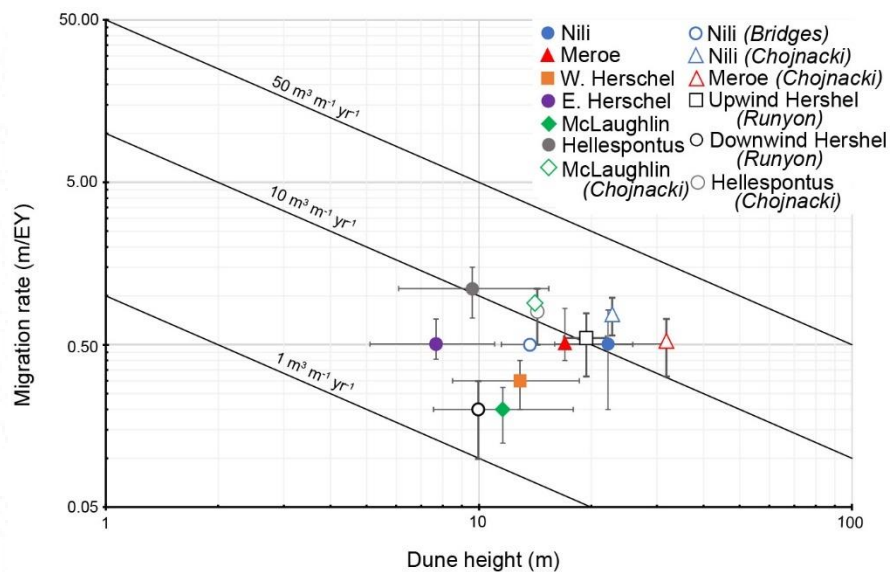


Figure 5: Log log plot showing the mean dune height versus migration rates for our six study sites and other select studies which used HiRISE data at the same sites. The HiRISE measurements are from: Bridges et al. 2012 (Nili Patera); Runyon et al., 2017 (Upwind and Downwind Herschel crater); Chojnacki et al., 2018 (Nili Patera, Meroe Patera, McLaughlin crater); and Chojnacki et al. 2019 (Hellespontus). The solid black lines show the sand flux at different rates (1 , 10 , and $5 \text{ m}^3 \text{ m}^{-1} \text{ EY}^{-1}$).

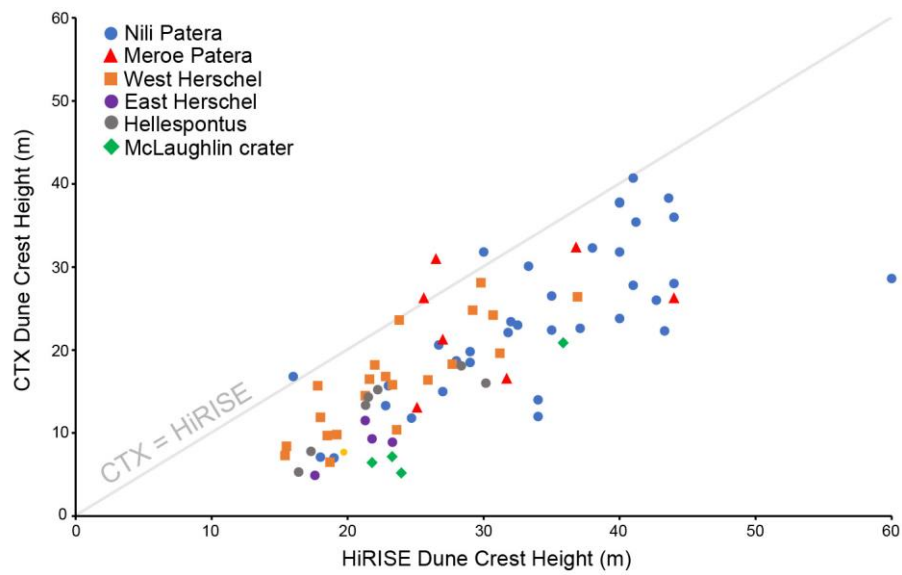


Figure 6: Comparison of dune heights extracted from HiRISE and CTX derived DEMs. The heights extracted from the CTX DEMs are typically less than the HiRISE heights.